# SANDIA REPORT

SAND2010-5430
Unlimited Release
Printed August 2010

# Photonuclear Activation of Pure Isotopic Mediums.

E. D. Lukosi, M. A. Grohman
Sandia National Laboratories

Prepared by
Sandia National Laboratories
Albuquerque, New Mexico 87185 and Livermore, California 94550

Sandia National Laboratories is a multi-program laboratory operated by Sandia Corporation, a wholly owned subsidiary of the Lockheed Martin Corporation, for the United States Department of Energy's National Nuclear Security Administration under Contract **DE-AC04-94AL85000**



Issued by Sandia National Laboratories, operated for the United States Department of Energy by Sandia Corporation.



Available to DOE and DOE contractors from
U.S. Department of Energy
Office of Scientific and Technical Information
P.O. Box 62
Oak Ridge, TN 37831

Telephone: (865) 576-8401
Facsimile: (865) 576-5728
E-Mail: reports@adonis.osti.gov
Online ordering: http://www.doe.gov/bridge

Available to the public from
U.S. Department of Commerce
National Technical Information Service
5285 Port Royal Rd
Springfield, VA 22161

Telephone: (800) 553-6847
Facsimile: (703) 605-6900
E-Mail: orders@ntis.fedworld.gov
Online order: http://www.ntis.gov/help/ordermethods.asp?loc=7-4-0#online

SAND2010-5430
Unlimited Release
Printed June 2010

# Photonuclear Activation of Pure Isotopic Mediums.

E. D. Lukosi, M. A. Grohman
Sandia National Laboratories
MS 1374
P.O. BOX 5800
Albuquerque, NM 87185-1374

## Abstract

This work simulated the response of idealized isotopic U-235, U-238, Th-232, and Pu-239 mediums to photonuclear activation with various photon energies. These simulations were conducted using MCNPX version 2.6.0. It was found that photon energies between 14-16 MeV produce the highest response with respect to neutron production rates from all photonuclear reactions. In all cases, Pu-239 responds the highest, followed by U-238. Th-232 produces more overall neutrons at lower photon energies then U-235 when material thickness is above 3.943 centimeters. The time it takes each isotopic material to reach stable neutron production rates in time is directly proportional to the material thickness and stopping power of the medium, where thicker mediums take longer to reach stable neutron production rates and thinner media display a neutron production plateau effect, due to the lack of significant attenuation of the activating photons in the isotopic mediums. At this time, no neutron sensor system has time resolutions capable of verifying these simulations, but various indirect methods are possible and should be explored for verification of these results.

# Contents

# List of Figures

# List of Tables

# Executive Summary

This work was conducted to cover actinide responses to photonuclear interactions. Photons of higher energy, in the range of 5-25 MeV interact with nuclei through the phenomena known as the Giant Resonances. This mechanism causes a large and broad increase in the photonuclear cross sections. The purpose of this report is to simulate the response of a select number of actinides to photonuclear interactions. The simulations were conducted using MCNPX 2.6.0 and post processing was conducted using Excel and Mathematica 7.0. In particular, the neutron production rates due to photonuclear interactions with an idealized isotopic material, each consisting of U-235, U-238, Th-232, and Pu-239 isotopes, was evaluated from both a time and non-time distributed source of photons. This work showed that the idealized Pu-239 material had the highest neutron production due to photonuclear activation with 7 MeV gamma rays, followed by U-238. U-235 produces fewer neutrons overall due to photonuclear activation by 7 MeV photons as compared to Th-232, but the reverse is true when higher energy gamma rays are used for photonuclear activation. The fact that more neutrons are created in Th-232 than in U-235 is also a function of material thickness, where 3.943 centimeter slab thickness is the dividing line. Also, in this high slab thickness, the neutron production decay is much longer than that of the other actinides, due to the significantly lower photonuclear attenuation coefficient of Th-232.

# Nomenclature

| | |
|---|---|
| ENDF | Evaluated Nuclear Data File |
| U-235 | Uranium-235 |
| U-238 | Uranium-238 |
| Th-232 | Thorium-232 |
| Pu-239 | Plutonium-239 |
| A | Atomic Mass Number |
| N | Number of Neutrons |
| Z | Atomic Number |
| IAEA | International Atomic Energy Agency |
| $S_n$ | Neutron Separation Energy |
| MCNPX | Monte Carlo n-Particle Transport Code |
| ps | $10^{-12}$ seconds |
| $\nu$ | Nubar or neutron multiplicity |
| $\mu_t$ | Time-Based Linear Photonuclear Attenuation Coefficient |
| $\mu_x$ | Linear Photonuclear Attenuation Coefficient |
| MeV | $10^6$ eV |
| eV | Electron Volt |
| d | Distance |
| v | Velocity |
| t | Time |
| c | Speed of Light |
| g | Gram |
| f | Fission |
| $\gamma$ | Gamma Ray |

# 1. Introduction

The idea of using photons to activate nuclei of interest is not a new concept. It has been studied by various groups over the years for reasons ranging from nuclear and elementary particle physics experiments trying to discover the underlying theories of matter to neutron sources and active interrogation of materials of interest. Most studies done in this area have not been thorough with respect to a certain class of isotopes. This is because baseline studies had not yet been conducted that identified and validated a set of photonuclear cross section libraries. Recently, however, the new U.S. ENDF/B-VII cross section library has been released, which includes some photonuclear cross sections [1]. This library is a verified compilation of nuclear cross sections from both theory and experiments and is contained within the National Nuclear Data Center at Brookhaven National Laboratory [2]. This study is concerned with the simulation of the response of select actinide isotopes to photonuclear reactions based upon these newly available libraries for a general study and reference of their expected response to high energy photons. The actinide isotopes of increasing interest in recent times will be simulated here, being U-235, U-238, Th-232, and Pu-239.

# 2. Basic Theory of the Nucleus

## 2.1 Nuclear Models

The nucleus of an atom is composed of protons and neutrons, which are held together by the strong force [3]. This force is the strongest in nature, and is only effective for very short distances, on the order of femtometers. The number of protons and neutrons in the nucleus is not random, as several factors must be taken into account. The first and most obvious is the separation of electronic charge. Neutrons seem to play the role of separating protons in the nucleus and adding increased strong force binding, allowing the nucleus to be stable. In addition, there seems to be some correlation between nuclei stability and whether there are an odd or even number of nucleons in the nucleus. There has also been an observation that there exist "magic numbers," where if the number of nucleons of either species in a nucleus is equal to one of these magic numbers, then the nucleus exhibits a strengthened stability. The simplest model of the nucleus comes from the liquid drop model. In this model, it is assumed that the nucleus acts as a liquid drop, meaning the occurrence of saturation of forces between its constituents. The theory produces a "semi-empirical mass formula" that describes the binding energy of the nucleus, and is based upon various terms such as volume, surface, and coulombic

effects [3,4]. This model has proven successful in this respect, being a description of the average behavior of the binding energy with mass number, but says nothing about other effects of the nucleus, such as magic numbers. This is what leads us to a different nuclear modeling approach, where the nucleons are assumed to be nearly independent of each other and in a common nuclear potential. The most successful models based upon this idea is the shell model.

The shell model assumes that the nucleons move freely in the nucleus, free from interactions with each other, much like the Fermi gas model. However, it is assumed that the particles are not free but are within a central potential field. The detailed theory is quite involved, but qualitatively, this concept is solved through adding a central potential field term in the Hamiltonian and that the residual contributions are zero. Assuming a simple harmonic oscillator yields the solution that gives rise to the concept of shells in the nucleus (through quantum numbers and degenerate states) and explains the first three magic numbers observed in nuclei. A more detailed discussion can be found in [4].

## 2.2 Nuclear Excitations

The activation methods of nuclei include nuclear excitation from both photons and particles, both charged and uncharged. Often, nucleonic interactions are indirect reactions, causing excitation from either inelastic collisions or absorption, where the responses of the nuclei are often characteristic of the target isotope [2]. Direct reactions can also occur, where nucleons are stripped off of the nucleus. However, this often requires large amounts of energy. Absorption increases the stored energy of the nucleus, where the added energy can lead to nucleonic emission and, in some cases, to nuclei dissociation, or fission [3].

Photonuclear excitation includes both direct and indirect reactions. Direct reactions consist of spallation, which requires tens of MeV or more of energy for most nuclei. Indirect excitation occurs when the electromagnetic radiation interacts with the protons in the nucleus. Based upon the shell model, the photon must bring enough energy into the nucleus to cause a quantum energy change. A strong sharp increase in the photo-absorption cross section is observed when the energy of the incident photons are slightly above the binding energy of a nucleon, and this excitation usually results in gamma ray release for de-excitation. However, when the energy of the photons are in 15-25 MeV range, a strong and broad increase in the absorption cross section is observed [4]. This phenomenon is called the Giant Resonance, where bulk motions of nucleons are observed, so that individual particle interactions and motions do not play a significant role in this phenomenon [5]. There are several kinds of resonances from photon absorption, which are classified through the change of their multipolarity (angular momentum), L, spin, S, and isospin, T, quantum numbers [5]. The first to be discovered is called the isovector giant dipole resonance, which corresponds to the photon imparting one unit of

angular momentum (ΔL=1) and isospin (ΔT=1) with no change in spin (ΔS=0). [4,5]. The qualitative reasoning behind this theory is two-fold, each of which fails to completely describe the phenomenon. The first assumes that nucleons are incompressible, and that a group of protons, after being photonically excited, oscillate out of phase with a group of neutrons, which intermix during the oscillation process. This theory predicts that the giant dipole resonance excitation energy varies as $A^{-1/6}$, where A is the atomic mass number of the target nuclei. The second theory assumes that the nucleons are compressible, and that photonic excitation causes density function variations with respect to time across the nucleus, where at a given instant the proton density will be higher on one side of the nucleus and the neutron density will be higher on the other side. This theory predicts that the excitation energy of the giant dipole resonance varies as a function of $A^{-1/3}$. However, combining these two theories gives the best approximation for the determination of the giant electric dipole excitation energy,

$$E_{GDR}(MeV) = \frac{112}{\sqrt{A^{2/3}+(A_o A)^{1/3}}}$$

where $A_o \cong 274$. This equation gives a good approximation to experimental data except for a few light atoms [4]. The strength of this giant dipole resonance can be described through the nuclei's total absorption cross section, found to be

$$\sigma_\gamma^{abs} = \frac{60NZ}{A}(1+k)\ mb \cdot MeV$$

where k is a factor due to meson-exchange contributions characteristic of all isovector resonances, typically 0.1 to 0.2 [4,5]. The isoscalar giant quadrupole resonance is described by the same process as the dipole resonance above, except that two units of angular momentum are imparted to the nucleus and no units of isospin is imparted. The isoscalar monopole resonance is interesting in that no angular momentum units are imparted to the nucleus. A plot of these three electric giant resonances is given in Figure 1.

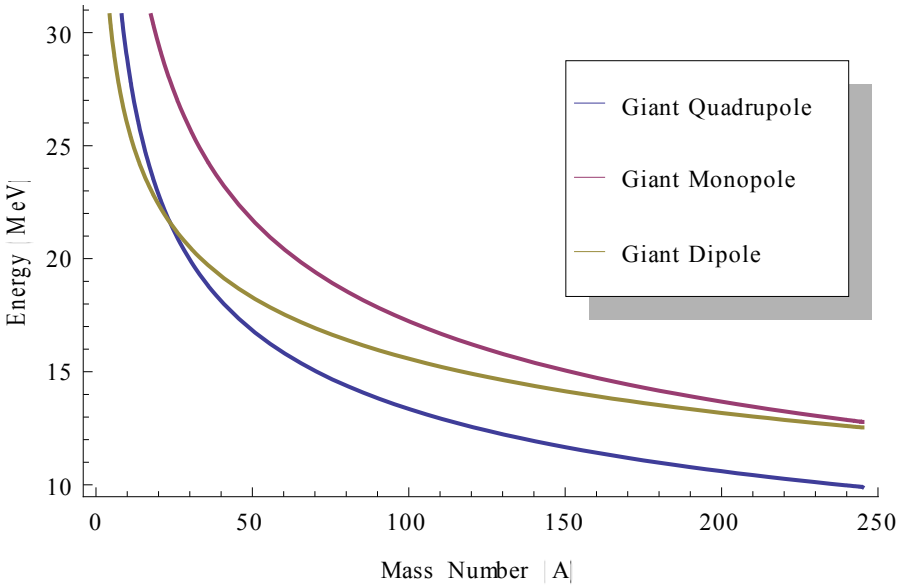


**Figure 1: Giant resonance excitation energies.**

The decay of these giant resonant states is important and can be numerous. The energy of these resonances is large and therefore many reaction paths exist. The possibility of gamma ray decay is generally accepted to decrease with increasing gamma ray energy, but that at energies around the isovector giant dipole resonance, there is an enhancement of this decay channel. However, the giant resonance energy region is above both the fission and neutron emission energy thresholds for all actinides. The giant resonance region of interest is between 8 and 14 MeV, where the energy widths of these resonances are around 3 MeV for heavy nuclei [5]. With this in mind, both neutron decay and fission are feasible decay mechanisms for U-238, where other actinides have similar qualities.

With this theoretical base, the question now is exactly what response will an actinide material give when exposed to higher energy photons. The national nuclear data center has recently released cross section tables for photonuclear reactions in the ENDF/B-VII library release. The IAEA have had unverified photonuclear cross section tables for the last several years, and new physics models exist that can approximate the response of isotopes due to photonuclear reactions. However, even with the release of these photonuclear cross section tables, there has yet to be a study of the response of actinides to photonuclear interactions for a general purpose overview and reference guide. It is the purpose of this report to provide this study.

# 3. Actinide Response to Photonuclear Interactions

## 3.1 System Parameters

The purpose of this study is to model the response of a few actinides in an ideal situation from exposure to photon radiation of varying energy. The control variables will be the energy of the activating photons and the isotopic material modeled. For simplicity, the actinides to be modeled will be assumed to be pure isotopic mediums, an idealized situation. This will allow for extrapolation of these results for any material of interest based upon this idealized study. To activate an isotopic medium, which will give characteristic responses due to the interactions with gamma rays, minimum energy thresholds for the activating photons need to be met. The energy required to strip a neutron off of a few actinides of interest along with their associated photofission threshold energies are listed in Table 1. This table indicates that neutron emission due to photonuclear reactions will compete with photonuclear fission. The photon energies to be used in this model are in the range of 7 to 20 MeV. Photonuclear cross section reactions for the isotopes listed in Table 1 are displayed in Figures 2 through 5.

**Table 1: Isotopic Photonuclear Characteristics**

| Isotope | $S_n$[a,b] (MeV) | Fission threshold energy (MeV) |
|---|---|---|
| $^{232}$Th | 6.44 | 6.0[c] |
| $^{235}$U | 5.29 | 5.8[d] |
| $^{238}$U | 6.15 | 5.8[e] |
| $^{239}$Pu | 5.65 | 5.8[f] |

[a] $S_n$ is the neutron energy separation from the nucleus.
[b] Data obtained from Jerome M. Verbeke *et al.*, UCRL-AR-228518 (2010).
[c] Data obtained from H. Schwoerer *et al*., Europhys. Lett., 61 (1), pp. 47-52 (2003).
[d] J. L. Caldwell *et al.*, Physical Review C, 21 (4), pp. 1215-1231 (1980).
[e] Data obtained from [4], pp. 405.
[f] B. L. Berman *et al.*, Physical Review C, 34 (6), pp. 2201-2214 (1986).

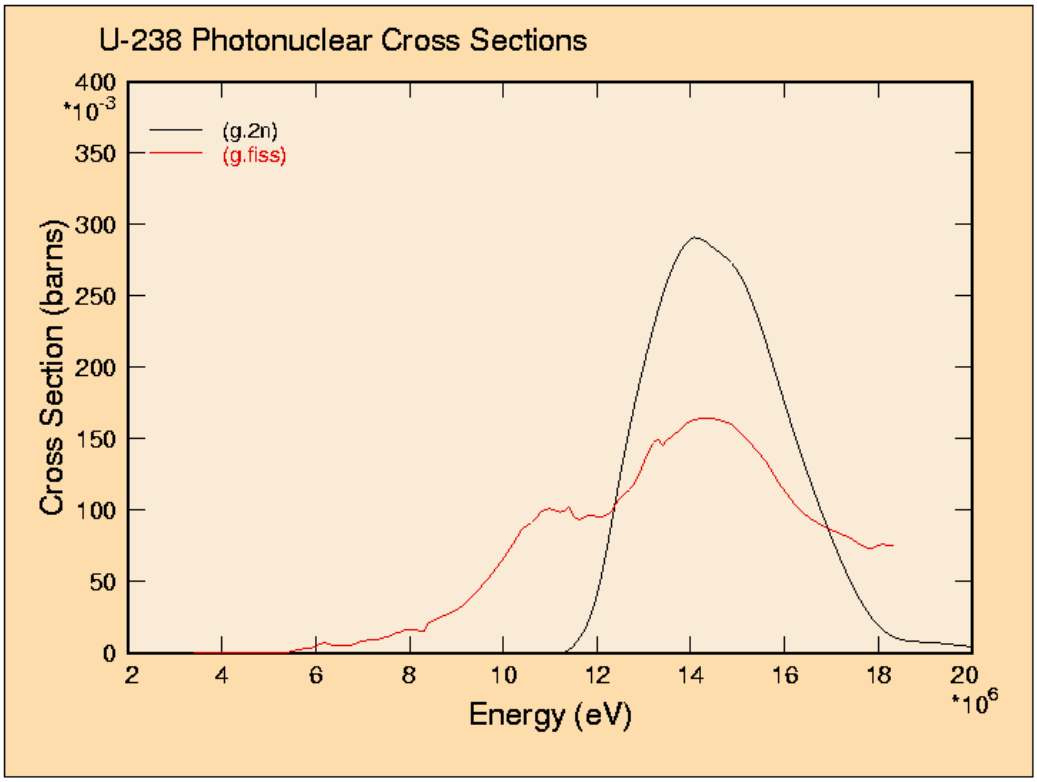


**Figure 2: Uranium 238 select photonuclear cross sections.**

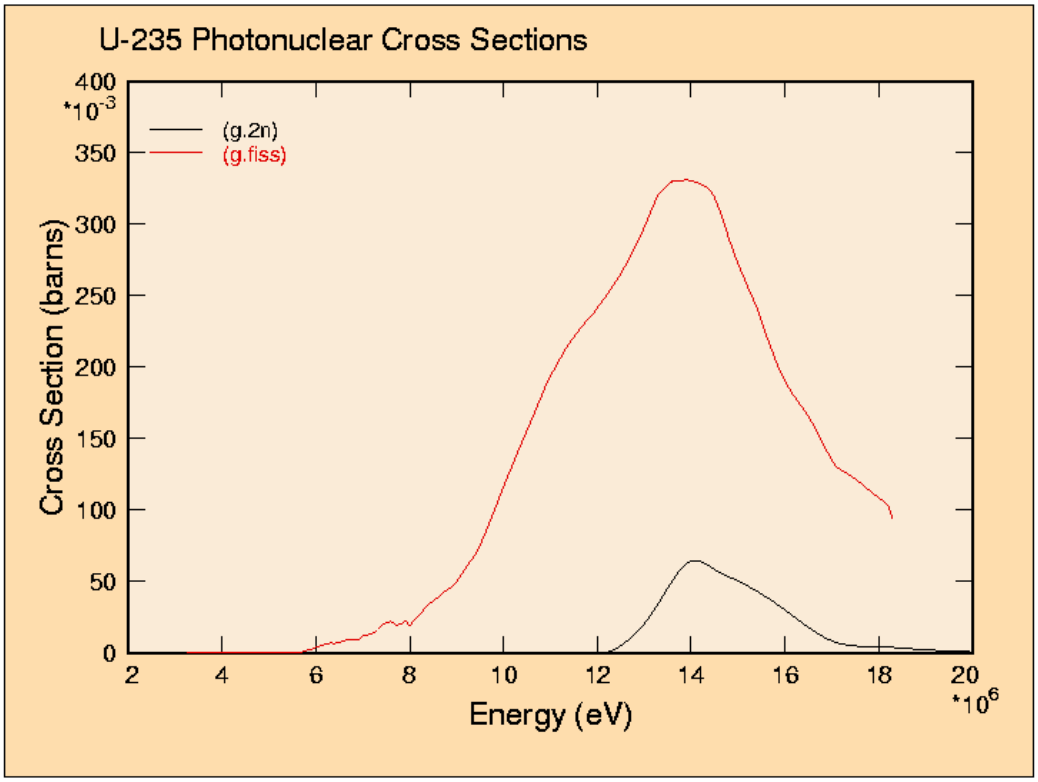


**Figure 3: Uranium 235 select photonuclear cross sections.**

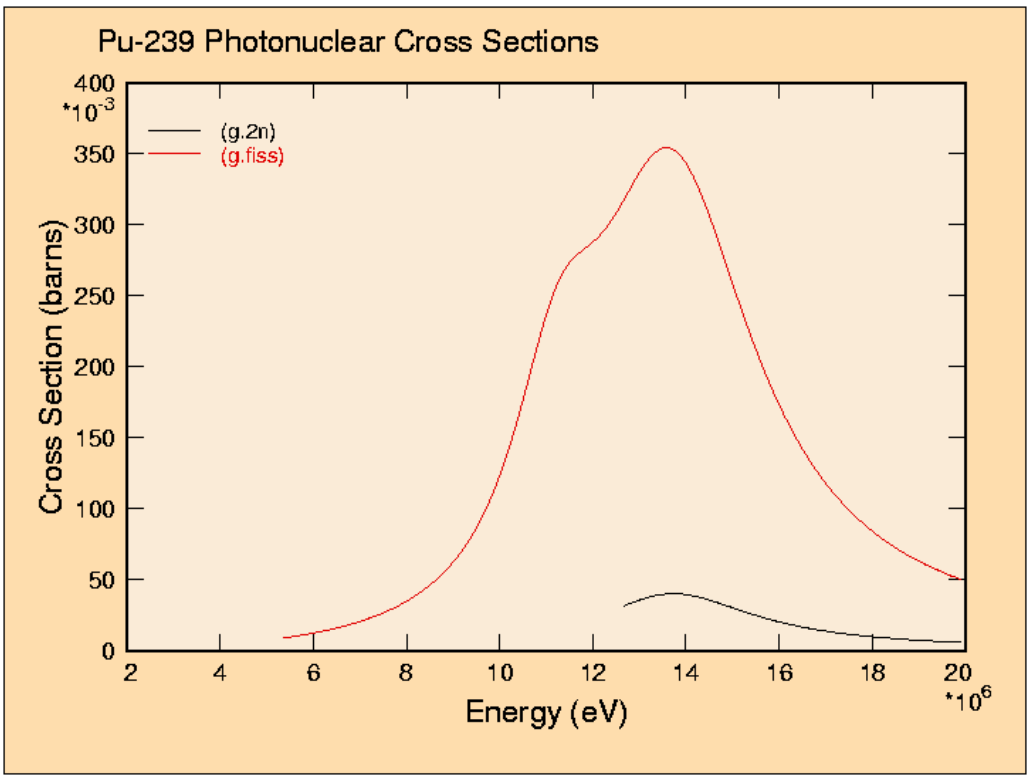


**Figure 4: Plutonium 239 select photonuclear cross sections.**

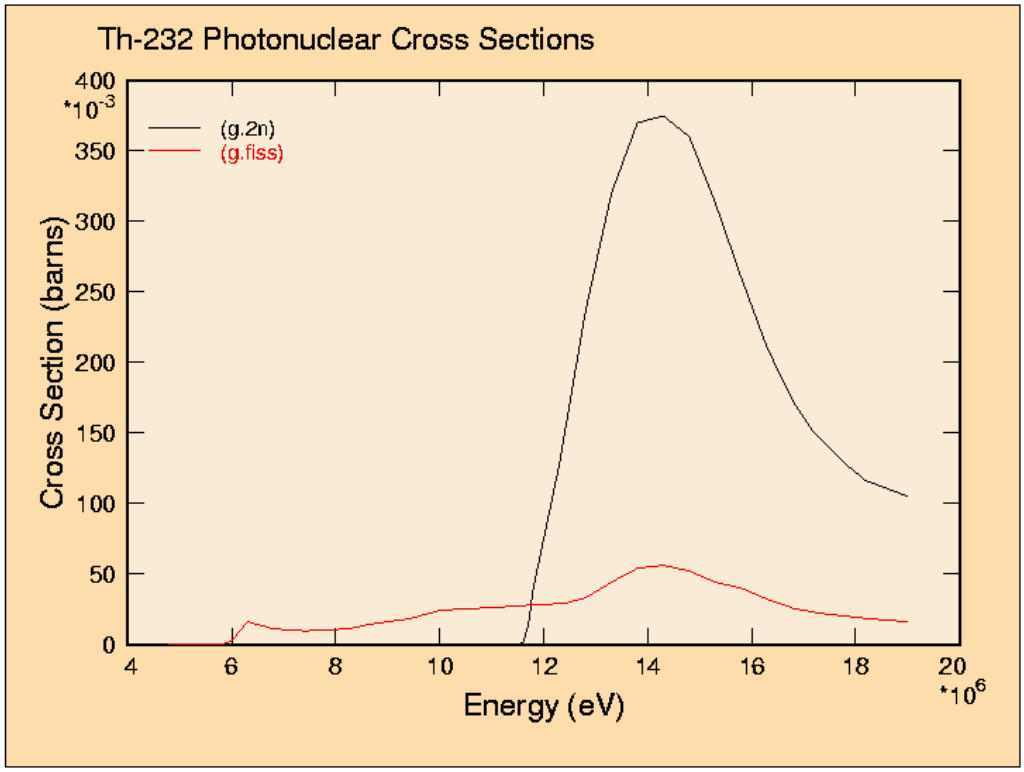


**Figure 5: Thorium 232 select photonuclear cross sections.**

## 3.2 Simulation Method

This project utilizes the MCNPX 2.6.0 software package. Several simulations will be conducted, where the beta photonuclear cross-section data from the MCNPX development team were used [6]. However, these cross-section tables do not contain data on Th-232 cross-sections with respect to photonuclear interactions, so the IAEA cross-sections were added to the libraries for photonuclear simulation of this isotope [7]. The isotopic medium modeled is assumed to be rectangular parallelepiped with dimensions of ten centimeters square by one centimeter thick. The program assumes a mono-directional plane source of photons and a void for all cells except for the one containing the isotopic medium. This is to give outputs that are based upon the number of photons incident, which is equal to the number of source particles, or histories, ran in the simulation. This will allow anyone to take the simulation results and adapt them to the number of source particles in their experiment or geometry of interest through geometrical efficiency concerns, where the source must be far from the material as the gamma ray source modeled here is mono-directional. Figure 6 gives a depiction of the system geometry. The source particles all start at zero time, so a non-time distributed source. The plane source of source particles is exactly 2.9989 centimeters away from the surface of the isotopic material. The program is designed this way so that it will take exactly 100 picoseconds before the source particles reach the surface of the isotopic medium. The data collected from this simulation type is used to integrate the response of the isotopic material to extrapolate the response of the material to a continuous work source of photons through post processing in Excel and Mathematica 7.0. Finally, a variable energy source is simulated here to give the reader an idea of the response of the isotopic materials with differing source particle energies, characteristic of the Giant Resonance phenomena discussed in section 2.2.

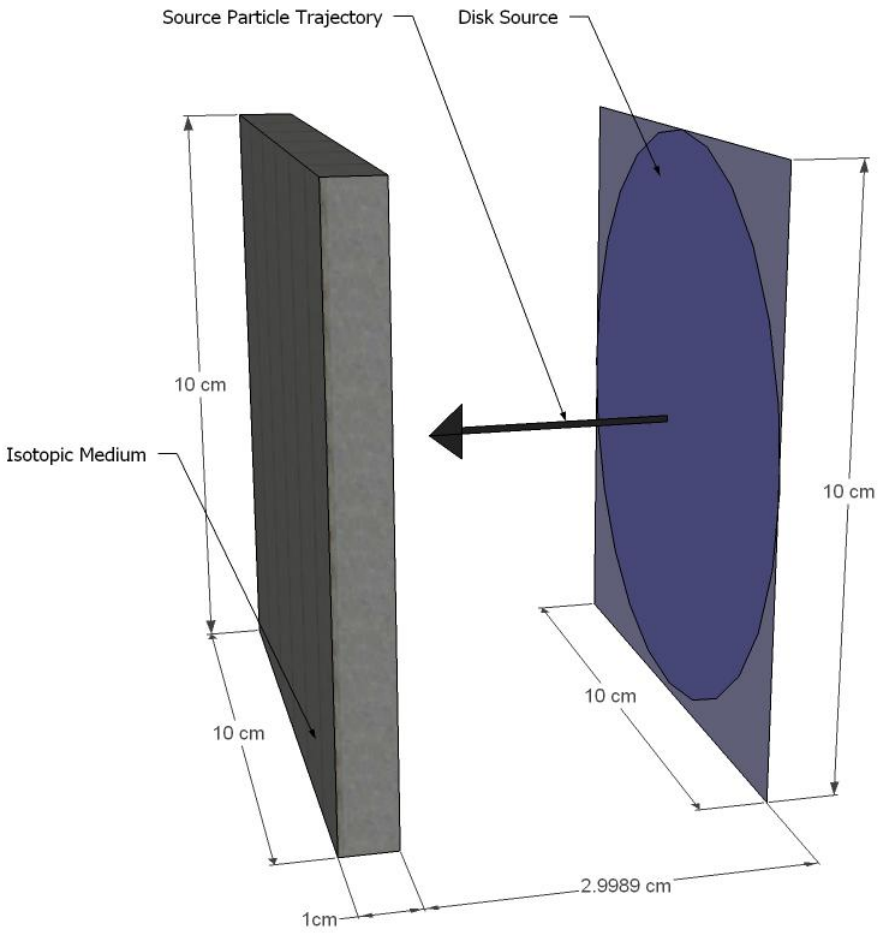


**Figure 6: System geometry for isotopic material modeling.**

# 4. Results and Discussion

## 4.1 Single Energy Photonuclear Response

The basic structure of the MCNPX program used in this analysis is given in Appendix A. Two simulations were conducted for each isotope listed in Table 1. The first simulation was for the response of the isotopic material from a source of gamma rays that are all emitted at zero time. The tally used in this simulation was the neutron production due to any neutron producing photonuclear reaction. Time tally bins were created with a fine mesh to determine the material response with high time resolution during the photonuclear interaction time. This data was exported for post processing into Mathematica and/or Excel for plotting purposes. The neutron production per source gamma ray from photonuclear reactions as a function of time is given in Figure 7 for the four isotopes of interest here.

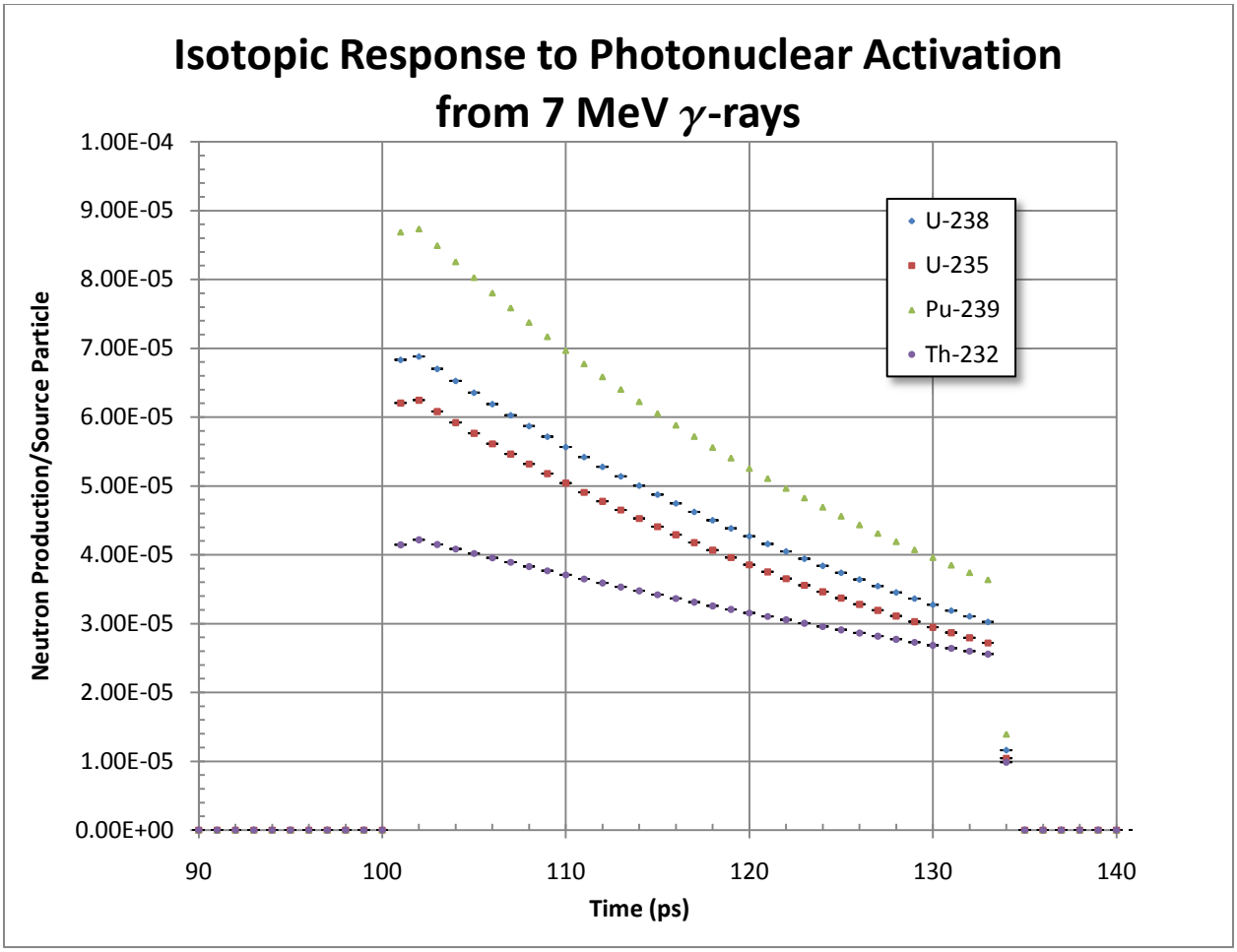


**Figure 7: Response curves from $(\gamma,\sigma_{tot})^*\nu$ interactions with 7 MeV gamma rays.**

From this Figure, it is obvious that interactions start after 100 picoseconds. This is due to the fact that the plane source of gamma rays is 2.9989 centimeters away from the surface of the isotopic material. Once the gamma rays reach the surface of the isotopic material, the photonuclear reactions start to take place, where the initial response is large but not the highest level response. At 102 picoseconds, the gamma rays are in the material long enough to reach their peak interaction probability. It is apparent from the plotted data that Pu-239 responds the highest to photonuclear activation from a non-time distributed gamma ray source with respect to neutron production, then U-238, followed by U-235, and finally Th-232.

After the initial response to the source of gamma rays, the response decreases exponentially and is caused by the attenuation of the gamma rays in the actinide material. Notice that 33 picoseconds after the gamma ray source particles enter the material, the neutron production rate drops to essentially zero in two picoseconds. This can be explained by basic arithmetic. Notice that the speed of light in any medium is less than the speed of light in a vacuum. Assuming that the index of refraction of all the idealized isotopic medium's is one, the time it takes for light to travel one centimeter is 33.35 picoseconds, and is the same amount of time it takes the light to travel across the isotopic slab of material, also being one centimeter thick. By looking at Figure 7 it is apparent that, after 33 picoseconds, the neutron production rate drops rapidly to zero, with a value about one half the value of the previous point at 34 picoseconds and the subsequent points giving neutron production rates of essentially zero. The reason the value of the data points displayed at 134 picoseconds for all actinide slabs does not follow the exponential trend is a construct of the way the MCNPX simulations were ran and the time bin construction for data tallying purposes. This is the same reason why the first data point in the actinide response to gamma ray activation does not follow the general data trend, because the time bin corresponding to the 100 to 101 picosecond bin does not have an entire picosecond of gamma ray interaction time for its tally, yielding a lower neutron production value than the subsequent point. However, the general data trend gives an accurate depiction of the actual neutron production in the slab with respect to time and is believed to accurately describe all four actinide material responses past the data point range. An exponential fit to the data curves in Figure 7 is supplied in Figure 8, where only the smooth exponential like decay is used for the fit. The exponential equation assumed for each curve fit is of the form

$$x(t) = Ae^{-\mu_t(t-x)}, \qquad 1$$

where A and $\mu_t$ are constants determined from the curve fit and x is the variable that shifts the curve left or right. Here, x is equal to 102 picoseconds, as this is the time it takes for the gamma rays to reach the actinide slab when emitted at zero seconds. The constant A represents the maximum neutron production value at the top of the curve and $\mu_t$ can be thought of as the time-based photonuclear attenuation coefficient, which is clarified as follows.

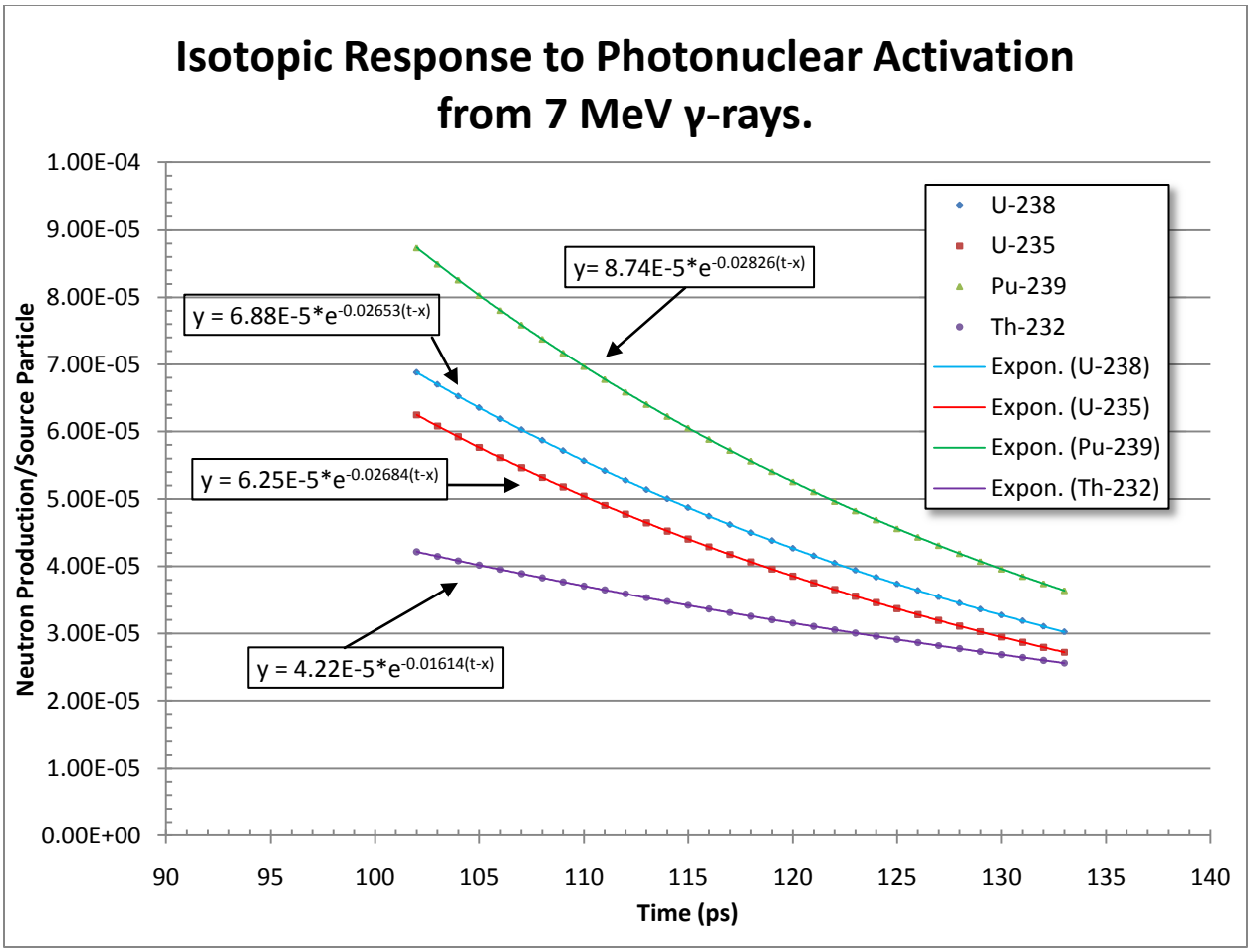


**Figure 8: Exponential trend lines from ($\gamma$,$\sigma_{tot}$)*$\nu$ interactions with 7 MeV gamma rays.**

In this simulation, all of the gamma rays are emitted at zero time. This means that all of the gamma rays will reach the isotopic medium wall at the same time and through the gamma ray interactions with the isotopes, at each time step into the simulation, there will be a change in the number of gamma rays that reach the next unit step of depth into the material, where a unit step of depth here is defined by the distance traveled by light in one picosecond, about 0.03 centimeters. Therefore, at each picosecond advance into the simulation the number of gamma rays still propagating through the material decreases proportionally with respect to the interaction probability with the material. The curve fit is with respect to time, but since all the gamma rays are emitted with no time distribution, the corresponding $\mu_t$ coefficient can be easily translated into a distance based linear photonuclear attenuation coefficient. This is done through utilizing the well-known equation d=vt, where d is distance, v is speed, and t is time. By solving for time and plugging this into our exponential curve fits, we see that the linear photonuclear attenuation coefficient, $\mu_x$, is equal to the time-based photonuclear attenuation coefficient divided by the

speed of light. Solving for $\mu_x$ for each of the four curves shown in Figure 8 yields the values given in Table 2.

**Table 2: Determined Linear Attenuation Coefficients at 7 MeV**

| Isotopic Medium | $\mu_t$ ($ps^{-1}$) | $\mu_x$[a] ($cm^{-1}$) | $\mu$[b] ($cm^{-1}$) |
|---|---|---|---|
| U-235 | 0.0268 | 0.895 | 0.904[c] |
| U-238 | 0.0265 | 0.885 | 0.904[c] |
| Pu-239 | 0.0283 | 0.942 | - |
| Th-232 | 0.0161 | 0.538 | 0.551[c] |

[a] This term represents the linear neutron production attenuation coefficient calculated in this work.
[b] This term represents the standard linear attenuation coefficient.
[c] Stephen Seltzer, NIST Standard Reference Database 126, Ionizing Radiation Division (July 2004).

From the data contained in Table 2, it is apparent that the method used here for determining the linear photonuclear attenuation coefficients have given values within one percent for uranium and four percent for thorium with respect to the linear attenuation coefficients listed through NIST (National Institute of Standards and Technology). However, a linear attenuation coefficient for plutonium could not be found and therefore, there is no basis for comparison with the determined value here. It is interesting to note that for the three isotopic mediums that have values for comparison, the calculated linear photonuclear attenuation coefficients here are all lower than their corresponding "standard" linear attenuation coefficients. The theory of calculating the mass attenuation coefficients, and therefore the linear attenuation coefficient, follow the general equation

$$\frac{\mu}{\rho} = \frac{\sigma_{tot}}{uA}$$

where $\rho$ is the density of the material, $\sigma_{tot}$ is the total gamma ray cross section per atom, u is the atomic mass unit ($1.66054*10^{-24}$ g), and A is the relative atomic mass of the target. The total gamma ray cross section includes the interactions from the photoelectric effect, Rayleigh and Compton scattering, pair production cross sections dependent on both the fields of the nucleus and the atomic electrons, and photonuclear cross sections. The exponential decay constant $\mu_x$ calculated here is proportional to the energy dependent photonuclear cross sections that produce neutrons and $\mu$ is proportional to the total cross section that removes gamma rays from an incident beam traveling through a material. This means that the removal of gamma rays should be higher when accounting for all removal mechanisms than when just considering photonuclear reactions, and this is what we see. However, the energy of the incident gamma rays decreases as they interact and down scatter in energy. This changes the photonuclear cross section for neutron production and therefore, this simulation includes neutrons produced through photonuclear reactions from lower energy gamma rays as well. Based upon the introductory talk on giant resonances and the photonuclear cross sections displayed in Figures 2 through 5,

however, it can be inferred that the contribution of neutron production by lower energy gamma rays is an order of magnitude or more lower and can essentially be ignored. To justify this statement, MCNPX simulations were ran to give the overall neutron production per source particle due to gamma rays in energies ranging from 1 to 20 MeV. Bar charts of these results for each of the four actinides modeled here are given in Figures 9 through 12. From these figures it can be seen that the response of any of the four actinides considered is significantly lower for energies below 7 MeV than at 7 MeV. It is also apparent that the energy used here produces a response much lower than could be induced if higher energy gamma rays were used for the photonuclear activation, where Figures 9 through 12 all indicate that the maximum response to photonuclear activation is between 14 and 16 MeV. The full width at half maximum for each plot is around 7 MeV, and indicates that the summed effect from each giant resonance type broadens the energy at which photons can be used for activation of these isotopes, as the electric dipole resonance has typical peak widths of 3 MeV, as discussed in section 2.2.

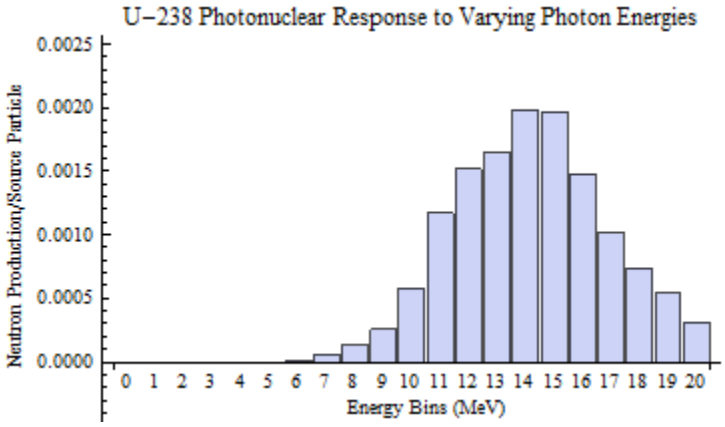


**Figure 9: U-238 (γ,f) Neutron Production Response to Various Photon Energies.**

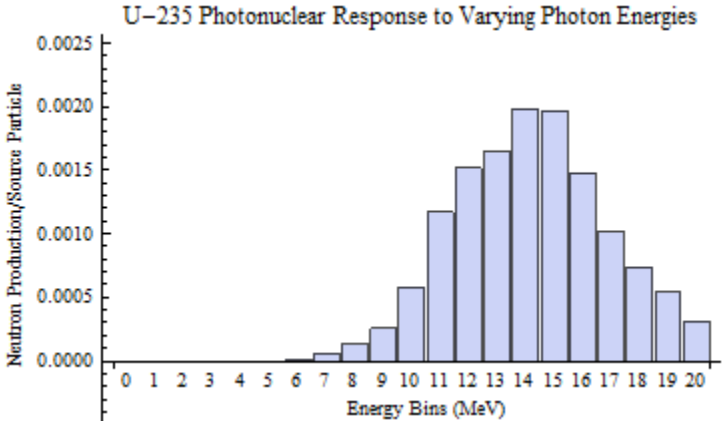


**Figure 10: U-235 (γ,f) Neutron Production Response to Various Photon Energies.**

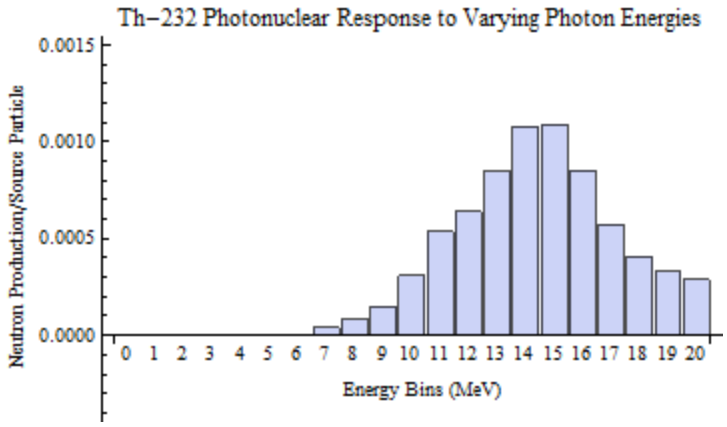


**Figure 11: Th-232 (γ,f) Neutron Production Response to Various Photon Energies.**

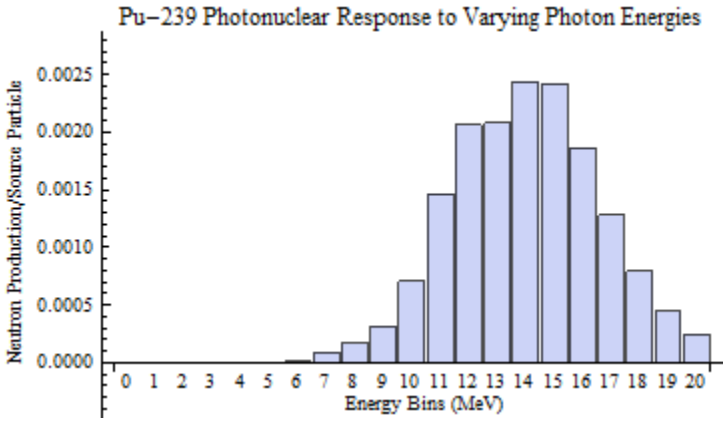


**Figure 12: Pu-239 (γ,f) Neutron Production Response to Various Photon Energies.**

With the results on the actinide responses to gamma ray energies, our calculated linear photonuclear attenuation coefficient is essentially for a gamma ray energy of 7 MeV only. It should also be noted that the curves used to calculate the linear photonuclear attenuation coefficient included not only the photonuclear reaction probability, but also multiplied by $\nu$, the neutron multiplicity for each corresponding photonuclear reaction. However, this is a constant for each photonuclear reaction and should not change the shape of the curve (the value of $\mu_t$), due to the low photonuclear interaction probability to create neutrons from photon energies below 7 MeV, but only the constant A in the exponential fit to the data.

## 4.2 Time Distributed Gamma Ray Source

Next the data from the MCNPX simulations on the actinide slab responses due to a 7 MeV gamma ray exposure was used to determine what the neutron production rate is due to a time distributed gamma ray source through post processing. The program used for data analysis is Mathematica 7.0. The fitted curves to the data given are in Figure 8 and were processed using Excel and Mathematica 7.0 as well. To simulate a time distributed source, a new function had to be defined based upon these curves. First off, the buildup of the neutron production rate with respect to time is of interest to us here. This can be shown directly through the data by assuming that the photonuclear activation response of each isotopic material is constant and the response curve is only shifted in time as the source gamma ray emission time is shifted. The data collected in the MCNPX simulations was broken up into time steps of ten picoseconds, the same time steps used for time binning the output data in the MCNPX simulations. Using Mathematica 7.0, the response curves of each material were time distributed and summed to estimate the actinide response due to a time distributed source. The result of this analysis is given in Figure 13.

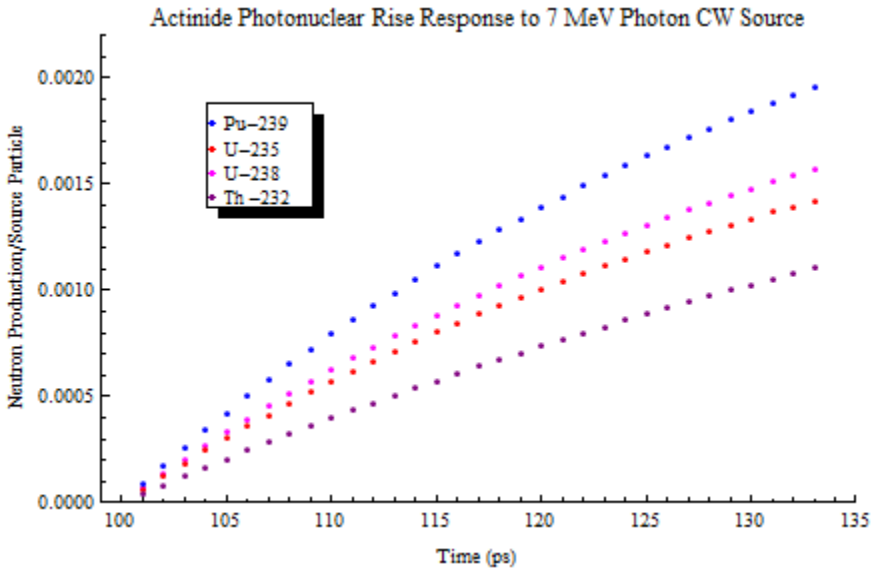


**Figure 13: ($\gamma$,$\sigma_{tot}$) *$\nu$ rise time curves from continuous work source.**

The time distributed response curve for each actinide displayed in Figure 13 does not extend past 134 picoseconds because of the system parameters chosen during modeling. The actinide slabs modeled were all chosen to be one centimeter thick. This thickness is low enough that a significant portion of the incident gamma ray beam gets through the isotopic medium. Because of this, the buildup of the neutron production plateaus, and the location of this plateau in time is directly proportional to the thickness of the slab. As an example, using the data collected

in the MCNPX simulations with a one centimeter thick isotopic slab and a 68 picosecond burst of gamma rays, the neutron production response of each isotopic material plateaus at 34 picoseconds after initial exposure and also takes 34 picoseconds for the plateau region to end. This is displayed in Figure 14.

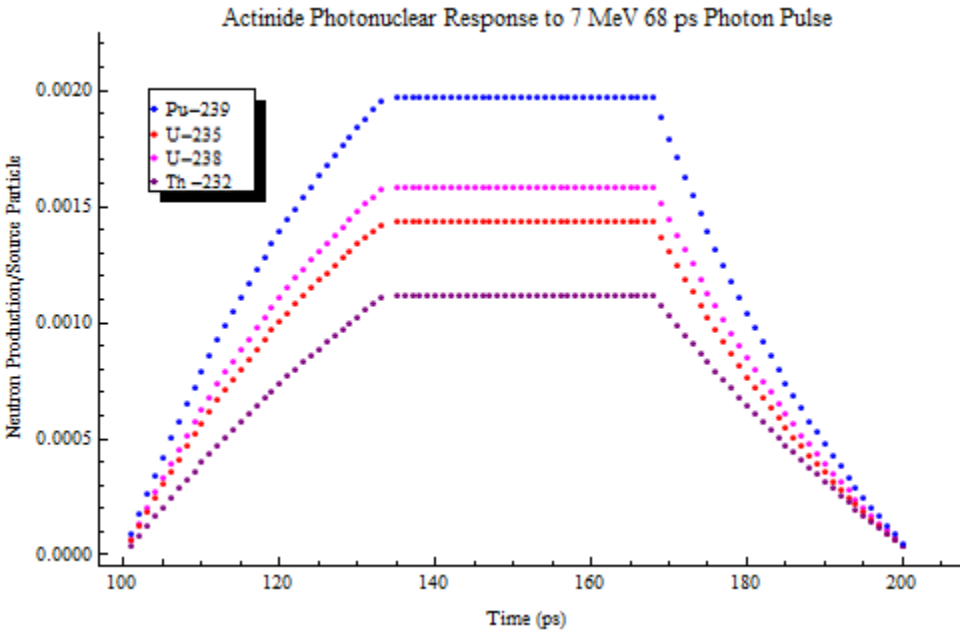


**Figure 14: Actinide ($\gamma$,$\sigma_{tot}$) *$\nu$ overall response curve from a 34ps pulsed source.**

To provide a more general picture with a greater control over the control variables of the problem, a general formulation of the collected output data is needed. To do this, the system parameters need to be identified. First off, the response of the material in time due to a non-time distributed gamma ray source is directly proportional to the thickness of the actinide slab. The thicker the slab is, the longer the gamma ray beam has to interact with the material and a larger overall neutron production results. The thickness of the actinide slab in every simulation was assumed to be one centimeter thick, but the exponential decay curve fit of the neutron production data fits very well, and so it is assumed that this trend line will be the same for any slab thickness. Furthermore, the response of the material only lasts as long as the gamma ray source is in the material, and so the function to be developed here had to be a function of slab thickness. Finally, the variable x displayed in the exponential decay function used to fit the MCNPX simulation data (see equation 1) is a variable here. This variable is used to define at what time gamma rays are emitted from the source, where it is assumed that a significant number of gamma rays are emitted at any time, otherwise the statistics of the Monte Carlo simulations do not give an adequate estimation of the response of the actinide materials and a transport method would need to be used. Based on these needs and assumptions, the following equation was developed

to represent the actinide slab response to photonuclear activation when the gamma rays are emitted at any time, represented by the variable x.

$$n(t,d,x) = Ae^{-\mu_t(t-x)}H[t-x]H[T(d)+x-t-2.3456] \quad 2$$

In equation 2, the independent variables are time, t, slab thickness, d, and gamma ray emission time, x. The constants A and $\mu_t$ have already been defined in Figure 8 and Table 2, and H[x] is called the Heaviside step function, defined below.

$$H[x] = \int_{-\infty}^{x} \delta(r)dr \quad 3$$

In this equation, it is shown that the Heaviside step function is the integral of the Dirac Delta function from negative infinity to some value x. What this means is that if x is less than r, then the integral is zero, but if x is greater than r, then the integral equals one. The two Heaviside step functions in equation two are essential for proper evaluation of our system. First, it takes time for the gamma rays to reach the actinide slab, and because of this the exponential equation describing the data is nonexistent until the gamma rays reach the slab. In this case, this time is equal to t-x, where x was equal to 102 picoseconds for the case of a non-time distributed source of gamma rays. Second, the gamma rays do no attenuate and interact indefinitely within the actinide slab, but instead the interaction time is a function of the actinide slab thickness, d. To accommodate this requirement, the second Heaviside step function is included in equation 2. This step function is a function of T(d)+x-t-2.3455. The subtracted constant 2.3455 is required because we assumed first gamma ray interaction occurs at 102 picoseconds (the value of x) where it actually starts at 100.3456 picoseconds, and so this addition ensures that the high side Heaviside theta function stops the exponential fit in equation 2 at the proper time. T(d) is the time length that the gamma rays interact with the actinide slab with the assumption that the index of refraction of each actinide material is unity. This is, of course, a function of distance, and using distance equals velocity times time, we see that

$$T(d) = \frac{d}{c}, \quad 4$$

where c is the speed of light. So the sum of T(d), x, and the constant 2.3455 is the time it takes for unattenuated gamma rays to reach the back side of the actinide slab. As long as it is less than this quantity, the Heaviside step function is one, but once it is above this value, the entire function in equation 2 is forced to zero.

Now that an equation describing our system has been defined, the overall response from a continuous work source of gamma rays was determined through integrating over the variable x from $t_o$ to $t_f$, where $t_o$ is the initial time of first gamma ray interaction and $t_f$ represents the time at which gamma rays are no longer emitted. Note that the actual gamma ray pulse is 102 picoseconds sooner than the time interval described here through $t_o$ and $t_f$, but this is necessary

due to the formulation used to describe our system. Note that $t_o$ here is one picosecond later than the actual time that gamma ray interactions score neutron production in the MCNPX simulations. The reason this is left out is to produce the best fit to the data possible, where this initial neutron production value is constant and is accounted for by just adding on this value to the final integrated equation 2. These values added on are given in Table 3 and are equal to the data points at 102 picoseconds in Figure 14. Also note the small data point value in Figure two at 134 picoseconds for all the neutron production actinide slab responses. This data point value is small and contributes little to the overall trend to the data. However, ignoring it completely systematically causes the estimated response curve to be lower than what the data suggests, but as the extrapolation goes farther and farther the error becomes less and less as the overall neutron production approaches it maximum value. Since we are concerned with time scales larger than a few picoseconds, this small contribution will be ignored. The integrated equation 2 is plotted against the MCNPX post processed data displayed in Figure 14 in Figure 15.

**Table 3: Added Values to Equation 2 for Exponential Fit of the Data**

| | U-235 $10^{-3}$ | U-238 $10^{-3}$ | Th-232 $10^{-3}$ | Pu-239 $10^{-3}$ |
|---|---|---|---|---|
| Values[1] | 1.372 | 1.245 | 0.836 | 1.743 |

[1] All value units are in neutron production/source particle

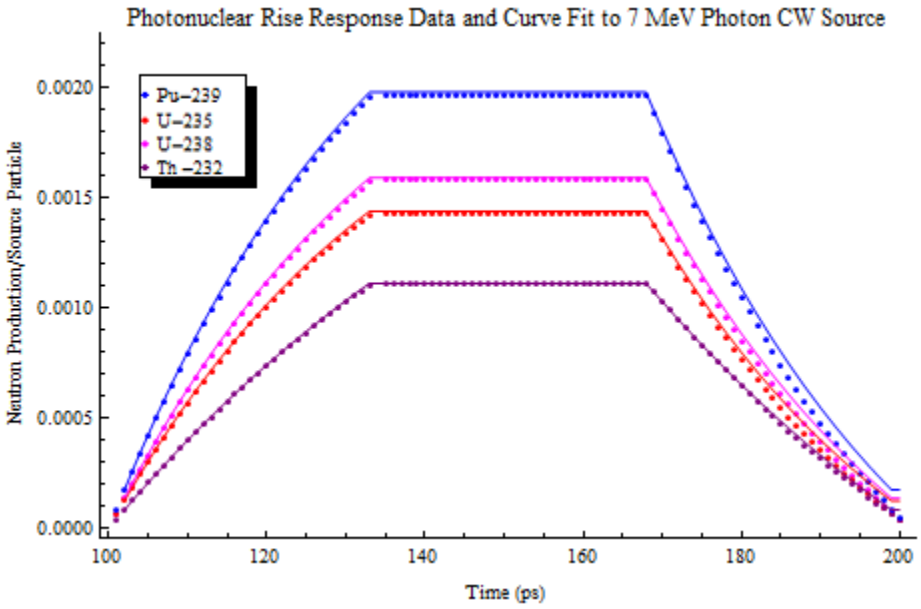


**Figure 15: Integrated exponential approximation plotted against the post processed data.**

From Figure 15, it is apparent that the defined function to describe the data fits very well and the only discrepancy is in the lower part of the decay curve for all the actinides, where the

formulation here slightly overestimates the neutron production at the end of the curve for all four actinide materials when compared to the data summation method. This formulation can be manipulated very easily to accommodate any slab thickness and gamma ray pulse time. As an example and to demonstrate the lack of a plateau effect with a slab of sufficient thickness, a plot of the four actinide materials is given in Figure 16 with a slab thickness of 10 centimeters with a gamma ray pulse time of 500 picoseconds.

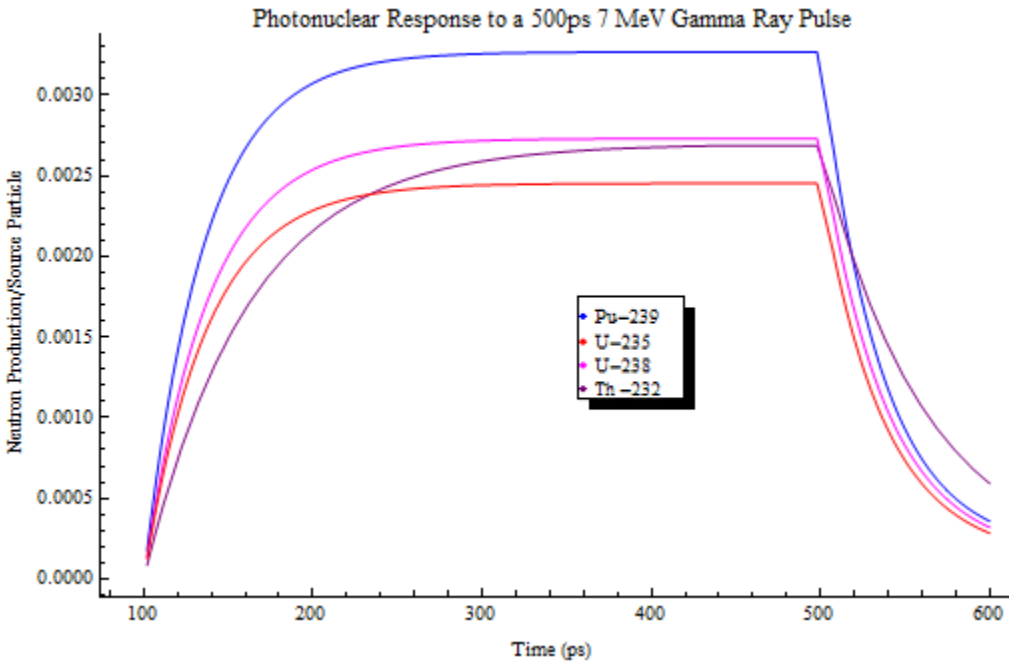


**Figure 16: Actinide Response Curves to a 500ps Gamma Ray Pulse**

There are some really interesting conclusions that can be drawn from Figure 16. First off, the buildup of the neutron production for each actinide occurs as it has in every other case considered here, such that Pu-239 has the highest response, followed by U-238, then U-235, and finally Th-232. However, as time goes on the total neutron production of Th-232 passes that of U-235 at 233.5 picoseconds and approaches the value of U-238. This is interesting in that the data in Figure 8 first suggests that this should not happen. However, if we integrate the fitted equations with no high side Heaviside step function, which is equivalent to an infinite slab thickness, and set x equal to 102 picoseconds, which represents a non-time distributed gamma ray source, along with adding the constant values from the first ignored data point in the exponential curve fit to the data, we see that the overall neutron production for Th-232 is higher than that of U-235 and is slightly lower than that of U-238. This can be explained through the lower value of $\mu_t$ as compared to the determined values for the other actinides, where the exponential decay of Th-232 is slower than that of the other three actinides modeled, and as such the area under the curve passes that of U-235 because they are initially so close. However, the

initial response of Th-232 is lower than that of the other three actinides and is due to its lower photonuclear stopping power with respect to the other actinides, but when a thick enough slab of Th-232 is present, the response of Th-232 becomes much stronger. This occurs when the material thickness of the actinide slabs is greater than 3.943 centimeters when the interrogating photon energy is 7 MeV. The values of the integration of the fitted exponential curves in Figure 8 used in the above analysis are given in Table 4. It must be noted that the response just described and displayed in Figure 16 is strongly dependent on the activating photon, which can be seen in Figures 2 through 5 and 9 through 12, and using a higher photon energy will allow the responses of the other three actinides to be significantly higher than the response of Th-232.

**Table 4: Integration of the fitted exponentials to the data in Figure 7.**

| | U-235 $10^{-3}$ | U-238 $10^{-3}$ | Th-232 $10^{-3}$ | Pu-239 $10^{-3}$ |
|---|---|---|---|---|
| Values[1] | 2.45 | 2.73 | 2.70 | 3.27 |

[1] All value units are in number of neutrons/source particle

Another interesting point is that the decay of the neutron production in time after the gamma ray pulse ends is less steep for Th-232 than for the other three actinides. Again, this is due to the significant difference in the value of $\mu_t$ for Th-232 versus the other three actinide materials. The curves in Figure 8 show that the neutron production does not decrease as much as the other actinides materials as the gamma rays travel through the Th-232 slab, due to Th-232's lower photonuclear attenuation coefficient. This means that neutrons will be produced for a longer period of time than the other actinide slabs because a larger fraction of gamma rays are still traveling in the Th-232 slab than in the other slabs in the same time period.

# 4. Conclusions

This study was concerned with the simulation of the photonuclear activation of four idealized, purely isotopic, actinide materials of interest, being Th-232, U-235, U-238, and Pu-239. The theory of giant resonances was touched on and simulations have shown that activation and subsequent neutron production through gamma ray exposure is feasible for energies between 7 MeV and 20 MeV. The simulations showed that Pu-239 produced the highest neutron production response, followed by U-238, and then either Th-232 or U-235, depending on the material thickness and activating photon energy. It was shown that the decay of neutron production in time from a non-time distributed gamma ray exposure is directly proportional to the photonuclear part of the linear attenuation coefficient for 7 MeV gamma rays, and that the contribution of lower energy gamma rays to the data curves was insignificant. The buildup of the neutron production in time was determined through post processing of the MCNPX

simulation data, and it was determined that a plateau region exists in the neutron production rate, which is caused by the finite thickness of the actinide materials modeled. Direct data point stacking and curve fitting were used to determine the response of the four idealized actinide materials to 7 MeV gamma ray exposures and the two methods agreed quite well. It was also shown that at 7 MeV, Th-232 produces more total neutrons than U-235, due to its larger photonuclear neutron producing cross sections at that energy. Using higher energy photons for activation will cause the total neutron production of U-235 to exceed Th-232 as the photonuclear fission cross section of Th-232 is relatively flat from 7 MeV to 19 MeV, where the photonuclear fission cross section of U-235 does not. Finally, because of the lower photonuclear attenuation coefficient of Th-232, the decay of neutron production after the gamma ray source is turned off is noticeably longer than that of the other actinide materials.

# 5. References


[1] M. B. Chadwick, *et al.*, ENDF/B-VII.0: Next Generation Evaluated Nuclear Data Library for Nuclear Science and Technology, Nuclear Data Sheets Vol. 107, pp. 2931-3060 (2006).

[2] M.-L. Giacri, *et al.*, Nuclear Sci. and Eng. 153, pp. 33-40 (2006).

[3] Stephen T. Thornton and Andrew Rex, *Modern Physics for Scientists and Engineers*, 3rd ed. (Tomson Brooks/Cole, Belmont, CA 2006), pp. 433-441, 454-455, 474-477.

[4] Carlos A. Bertulani, *Nucelar Physics in a Nutshell* (Princeton, New Jersey 2007), pp.119, 128-141, 307, 312-315.

[5] M. N. Harakeh and A. van der Woude, *Giant Resonances: Fundamental High-Frequency Modes of Nuclear Excitation* (Oxford, New York 2001), pp. 1-18, 405-408.

[6] Gregg W. McKinney, MCNPX Data Library, Los Alamos National Security (2009). https://mcnpx.lanl.gov/

[7] Handbook on Photonuclear Data for Applications: Cross Sections and Spectra, IAEA co-coordinated research project (IAEA-TECDOC-Draft No 3, March 2000).

# Appendix A: MCNPX Program

The program used in this simulation describes the system geometry displayed in Figure 6. A single tally was taken for this simulation, namely the neutron production rates in the isotopic cell from the (γ,f) photonuclear reaction. Time bins were made for this tally, where these time bins allow for inspection of the response of the SNM at specific time periods. The time bins for these tallies are not listed explicitly here, as the input is far too large. However, they can be interpreted though the plots provided in section 3.

Below is a copy of the MCNPX program used in the evaluations. Note that the "X" parts of the program points the user to Table 2 in Appendix A, which lists the card changes for each of the simulations. The "OMITTED" entry in the program is placed there to tell the user that items were deleted due to space concerns, due to the fact that over two-thousand entries exist for some simulations.

**Table 5: MCNPX program changes corresponding to differing isotopic mediums.**

| Isotope | Density ($g/cm^3$) | Material card Entry One |
|---|---|---|
| U-235 | -19.1 | 92235.70c 1 PNLIB=70u |
| U-238 | -19.1 | 92238.70c 1 PNLIB=70u |
| Th-232 | -11.7 | 90232.70c 1 PNLIB=.27u |
| Pu-239 | -19.8 | 94239.70c 1 PNLIB=70u |

```
Study on the response of pure isotopic samples to photonuclear activation
c
c
c   ***************************************************************************
c                                    CELL CARDS
c   ***************************************************************************
c
c   Below is the cell cards that describes the system at hand.  Cell one is the material of interest
c   being activated, cell two is a dummy cell used as a dummy cell for source reasons, and cell 3
c   is the rest of space and therefore, is given zero transport importance.
c
1   1 X  1  -2  3  -4   5  -6    IMP:N,P=1
2   0      -1   3 -4   5  -6   7    IMP:N,P=1
3   0       2:-3:4:-5:6:-7          IMP:N,P=0

c   ***************************************************************************
c                                  SURFACE CARDS
c   ***************************************************************************
c
c   Below are the surface cards used to define the cells.
c
```

```
1   PX  0
2   PX  1
3   PZ -5
4   PZ  5
5   PY -5
6   PY  5
7   PX -2.9989

c   ***************************************************************************
c                                   DATA CARDS
c   ***************************************************************************
c
c
Mode N P
c
PHYS:P 100 0 0 -1 1 -101
c
c
PHYS:N 100 0 0 -1001 -1 0 0
c
c
c   Below is the material card for the problem, which is the isotope of interest, with respect to
photonuclear activation.  The photonuclear library to be used here is the new MCNPX
photonuclear libraries (70u) or the IAEA libraries for Th-232 (27u).
c
c
M1   X
c
c
c   Below is the source card for this problem.  Note that this is for the single photon energy
c   problem, and for the simulation giving results over many photon energies, the following card
c   entries must be included, where the ERG option must be changed from 7 to D2.
c
c       SI2 1 2 3 4 5 6 7 8 9 10 11 12 13 14 15 16 17 18 19 20
c       SP2 0 1 1 1 1 1 1 1 1 1 1 1 1 1 1 1 1 1 1 1.
c
SDEF SUR=7 RAD=D1 DIR=1 ERG=7 PAR=2 TME=0 POS= - 2.9989 0 0
SI1 5
c
c
c   The following cards are to measure the neutron production rate from the various neutron
c   producing photonuclear reactions.  The Fm card below is for multiplying the f4 tally by the
c   appropriate values to obtain the desired results.  Here the -1 indicates multiplying by the atom
c   density and the SD4 1 is multiplying by the cell volume, and the 1 indicates this is for cell
c   one, and the 1001 indicates the total neutron production due to all photonuclear reactions.
c
```

```
c
FC4  (g,tot) * Rxn_XS * F14 * Volume * N(isotope).
F4:P 1
FM4 -1 1 1001
SD4 1
c
c
c    This is our time bin card to allow are tally information to be broken
c    up into time bins for post processing of the data.
c
c
T0   0.0090 0.0091 0.0092 0.0093 0.0094 0.0095 0.0096$
     0.0097 0.0098 0.0099$
     0.0100 0.0101 0.0102 0.0103 0.0104 0.0105 0.0106$
     0.0107 0.0108 0.0109 0.0110 0.0111 0.0112 0.0113$
     0.0114 0.0115 0.0116 0.0117 0.0118 0.0119 0.0120$
     0.0121 0.0122 0.0123 0.0124 0.0125 0.0126 0.0127$
     0.0128 0.0129 0.0130 0.0131 0.0132 0.0133 0.0134$
     0.0135 0.0136 0.0137 0.0138 0.0139 0.0140 0.0141$
     0.0142 0.0143 0.0144 0.0145 0.0146 0.0147 0.0148$
     0.0149 0.0150 0.0151 0.0152 0.0153 0.0154 0.0155$
     0.0156 0.0157 0.0158 0.0159 0.0160 0.0161 0.0162$
     0.0163 0.0164 0.0165 0.0166 0.0167 0.0168 0.0169$
     0.0170 0.0171 0.0172 0.0173 0.0174 0.0175 0.0176$
     0.0178 0.0179 0.0180 0.0181 0.0182 0.0183 0.0184$
     0.0185 0.0186 0.0187 0.0188 0.0189 0.0190 0.0191$
     0.0192 0.0193 0.0194 0.0195 0.0196 0.0197 0.0198$
     0.0199 0.0200 0.0201 0.0202 0.0203 0.0204 0.0205$
     1E+36
c
c
c     This card is used so that a mctal file will be created so we can
c     export the data into an excel file.
c
c
PRDMP 0 0 -2 0 0
c
c
c     Below is the number of particle histories that will be recorded.
c
NPS 10000000
c
c
PRINT -85 -86
```

# Distribution

**UNCLASSIFIED unlimited release documents:**

| | | |
|---|---|---|
| 12 | | University of Missouri-Columbia<br>Nuclear Science and Engineering Institute<br>Attn: Eric Lukosi (10)<br>Mark A. Prelas<br>Sudarshan K. Loyalka<br>E2433 Lafferre Hall,<br>University of Missouri,<br>Columbia, MO 65211 |
| 1 | | DTRA<br>Attn: Peter Zielinski<br>8725 John J. Kingman Road<br>Stop 6201<br>Fort Belvoir, VA 22060-6201 |
| 1 | | DOE/OSTI via URL |
| 1 | M1080 | M. S. Derzon, 17492 |
| 1 | M1374 | P. C. Bennett, 6723 |
| 1 | M1374 | M. A. Grohman, 6723 |
| 1 | M1212 | E. Padilla, 5935 |
| 1 | MS 0899 | Technical Library, 9536 (electronic copy) |